ELSEVIER

Journal of Power Sources 76 (1998) 116–123

JOURNAL OF POWER SOURCES

Short communication

A rechargeable solid-state proton battery with an intercalating cathode and an anode containing a hydrogen-storage material

Kamlesh Pandey, N. Lakshmi, S. Chandra *

Department of Physics, Banaras Hindu University, Varanasi 221 005, India

Received 28 May 1998; accepted 23 June 1998

Abstract

Rechargeable proton batteries have been fabricated with the configuration $Zn + ZnSO_4 \cdot 7H_2O//$solid-state proton conductor$//C +$ electrolyte + intercalating $PbO_2 + V_2O_5$. The solid-state proton conductor is phosphotungstic acid ($H_3PW_{12}O_{40} \cdot nH_2O$) or a $H_3PW_{12}O_{40} \cdot nH_2O + Al_2(SO_4)_3 \cdot 16H_2O$ composite. The maximum cell voltage is ~ 1.8 V at full charge. The cell can run for more than 300 h at low current drain (2.5 $\mu A\ cm^{-2}$). Further, the cell can withstand 20 to 30 cycles. The addition of a metal hydride in the anode side enhances the rechargeability and the addition of a small amount of $Al_2(SO_4)_3 \cdot 16H_2O$ in the $H_3PW_{12}O_{40} \cdot nH_2O$ electrolyte improves the performance of the battery.

Keywords: Rechargeable proton battery; Proton conductor; Anode; Cathode

1. Introduction

Extensive efforts have recently been directed towards the development of all-solid-state batteries, particularly in view of their possible advantages in terms of long shelf-life, less electrode corrosion, higher temperature range of operation, easy leakproofing/packing, etc. Attempts have also been made to obtain rechargeable solid-state batteries by choosing suitable reversible cathodic/anodic half-cell reactions [1,2]. One approach is to use a cathode consisting of intercalating layered material (TiS_2, PbO_2, V_2O_5, MnO_2, etc.) into or from which small ions can either be intercalated or de-intercalated during discharge and charge, respectively. The intercalation efficiency is generally high for small ions and thus Li^+ and H^+ ion based rechargeable batteries as prime candidates. There have been many studies of Li^+-based batteries because of the availability of good lithium ion conductors and a large electrochemical window [2,3]. In the last decade, many good proton conductors have also been developed and, hence, a commercially viable proton battery becomes a possibility [4–7]. The anode material of an ideal proton battery must be able to maintain a supply of protons (H^+). Such materials could be salt hydrates or metal hydrides [4,8,9]. The research reported here uses a lightweight metal hydride (Mischmetal-based hydrogen storage material) developed in our department [10]. Phosphotungstic acid ($H_3PW_{12}O_{40} \cdot nH_2O$) or $H_3PW_{12}O_{40} \cdot nH_2O + Al_2(SO_4)_3 \cdot 16H_2O$ composite is employed as a proton-conducting electrolyte. Although $H_3PW_{12}O_{40} \cdot nH_2O$ is a good proton conductor [11], it loses its water of crystallisation (i.e., source of H^+) very quickly with decrease in humidity and its pellitization leads to partial dehydration. The pellets obtained are often sticky. In order to overcome this problem, an attempt has been made to prepare composites of phosphotungstic acid with aluminium sulfate which is also a proton conductor, but a poor one [12]. Intercalating cathodes such as TiS_2, PbO_2, V_2O_5, MnO_2, etc. (used singly or in combination) were chosen for preliminary studies. More than 60 cell configurations were investigated. The present paper gives the typical characteristics for a few selected cells with the following configuration:

Anode $(A_1$ or A_2 or $A_3)$/Solid proton conductor $(SPC)_1$

or $(SPC)_2$/C + proton conducting electrolyte + V_2O_5

+ PbO_2

where: $A_1 = Zn$; $A_2 = Zn + ZnSO_4 \cdot 7H_2O$; $A_3 = Zn + ZnSO_4 \cdot 7H_2O$ + metal hydride; $(SPC)_1 = H_3PW_{12}O_{40} \cdot nH_2O$; $(SPC)_2 = xH_3PW_{12}O_{40} \cdot nH_2O + (1 - x)Al_2(SO_4)_3 \cdot 16H_2O$.

* Corresponding author. Fax: +91-542-317-074; E-mail: schandra@banaras.ernet.in

0378-7753/98/$19.00
PII: S0378-7753(98)00132-3

The results are given only for those cells for which the active intercalation material chosen is a mixture of two intercalating materials, viz., $V_2O_5 + PbO_2$, which give a relatively better performance. The best performance is achieved when V_2O_5 and PbO_2 are used as a mixture rather than separately.

2. Experimental

The materials employed were of analytical grade purity and used as supplied by the manufacturers. The hydrogen-storage material is mischmetal-based, aluminium substituted penta nickelide ($MmNi_{4.5}Al_{0.5}$) which was synthesised by a ball-milling technique as described by Singh et al. [10]. The $MmNi_{4.5}Al_{0.5}$ was exposed to hydrogen for 24 h to form a metal hydride.

Pellets of phosphotungstic acid and/or aluminium sulfate and the composite cathode were prepared at a pressure of about 2×10^3 kg cm^{-2}. The diameter of the pellet was 0.8 cm. Electrical conductivity studies were performed on the pellets by means of a Solartron Frequency Response Analyser 1250 with an electrochemical interface 1286 coupled to a HP computer. The frequency range was 65 Hz to 65 kHz. The measurements were performed on pellets of different composition.

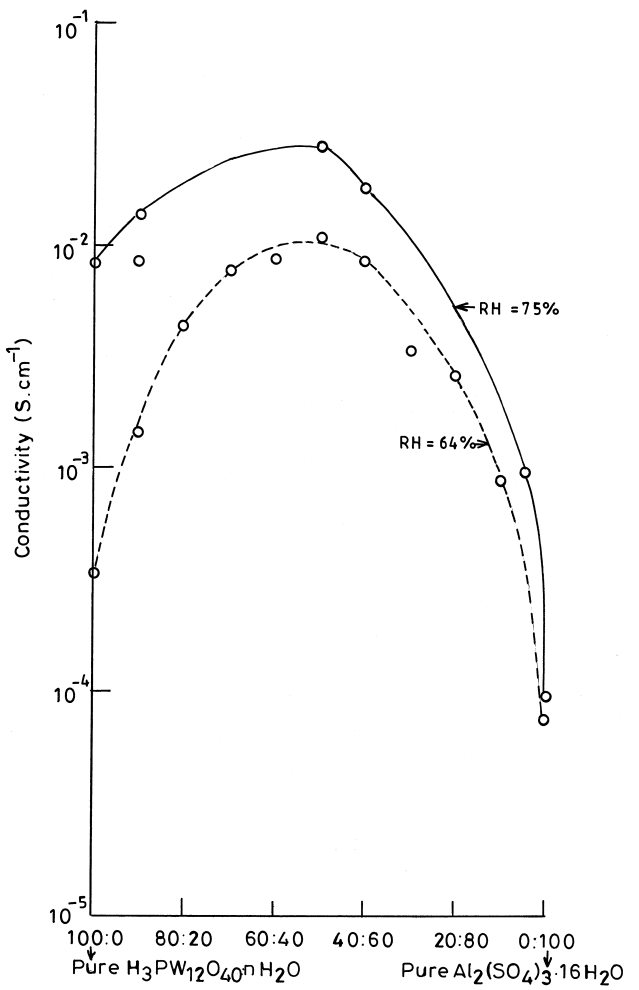

Fig. 1. Variation of conductivity with composition of $xH_3PW_{12}O_{40} \cdot nH_2O + (1-x)Al_2(SO_4)_3 \cdot 16H_2O$ composite electrolyte.

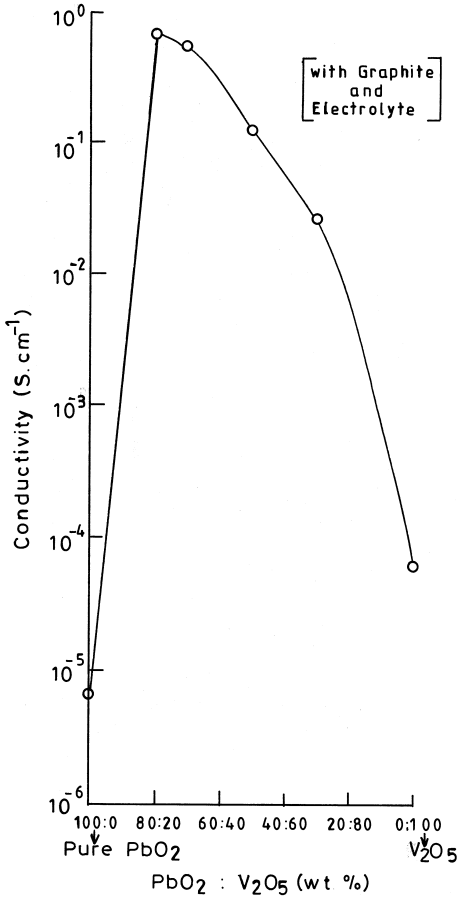

Fig. 2. Variation of conductivity with composition of intercalation cathode $xPbO_2 + (1-x)V_2O_5 + C + E$.

The integrated, solid-state, protonic battery was assembled by successively pressing the anode, electrolyte and the cathode compositions in the same pelletising die. At first, the desired anode was obtained by gently pellitizing the powders of A_1 (pure zinc) or A_2 ($Zn + ZnSO_4 \cdot 7H_2O$, 3:1 wt. ratio) or A_3 ($Zn + ZnSO_4 \cdot 7H_2O$ + metal hydride 10:3:1 wt. ratio). The electrolyte powder, viz., $(SPC)_1 = H_3PW_{12}O_{40} \cdot nH_2O$ or $(SPC)_2 = H_3PW_{12}O_{40} \cdot nH_2O + Al_2(SO_4)_3 \cdot 16H_2O$ (1:1 wt. ratio), was poured onto the compacted anode in the die and the assembly was again pressed gently. Subsequently, the cathode mixture (C + solid electrolyte + $V_2O_5 + PbO_2$) was poured into the die and pressed gently. The entire assembly was finally compacted at 3×10^3 kg cm^{-2}. The cell dimensions are: diameter = 0.76 cm; thickness = 0.50 cm.

Immediately after fabrication of the cell, the open-circuit voltage (OCV) was measured by a high impedance multimeter (Philips PM 2718). The cell was allowed to

stabilise for 8 to 10 h after which its voltage became constant. All studies (OCV, charge–discharge) reported in this paper were performed on such cells. The cell impedance/admittance was measured by drawing complex-impedance plots in the frequency range 0.1 Hz to 65 kHz.

3. Results and discussion

3.1. Conductivity of electrolyte and intercalating cathodes with composition

Electrical conductivity studies were undertaken to determine the optimum compositions of the electrolyte $xH_3PW_{12}O_{40} \cdot nH_2O + (1-x)Al_2(SO_4)_3 \cdot 16H_2O$ (where x = wt.% ratio) and the intercalating composite cathode. The variation of conductivity of the electrolyte as a function of composition is shown in Fig. 1. The conductivity increases initially with increase in the amount of $Al_2(SO_4)_3 \cdot 16H_2O$ admixed in phosphotungstic acid. It then attains a maximum and decreases. $50H_3PW_{12}O_{40} \cdot nH_2O + 50Al_2(SO_4)_3 \cdot 16H_2O$ is found to be the best conducting ratio of the composite electrolyte. The mechanism of enhanced ionic conductivity in the composites or dispersed phase systems is well documented [13]. The conductivity is ionic with $t_{ion} > 0.9$, as measured by Wagner's d.c. polarization method [14].

The variation of conductivity with composition of the composite cathode ($PbO_2 + V_2O_5 + C + E$) is shown in Fig. 2. The optimized composite cathode is $PbO_2 + V_2O_5$ (80:20 wt.%) and has good electronic conductivity which is a requisite criterion for cathodes.

3.2. Discharge characteristics

The discharge characteristics of some typical cells at three different loads are given in Fig. 3. When discharged with low load (resistance 50 kΩ and 10 kΩ), the voltage–current curve exhibits a rapid initial fall and then remains stable (within 5% of the voltage after initial drop) for a few hours. Subsequently, it starts to decrease rapidly. The data in Tables 1 and 2 show how the cell performance is affected by changing the electrolyte and/or the anode composition. It is clear from Table 1 that with the same anode composition (Zn or $Zn + ZnSO_4 \cdot 7H_2O$ or Zn +

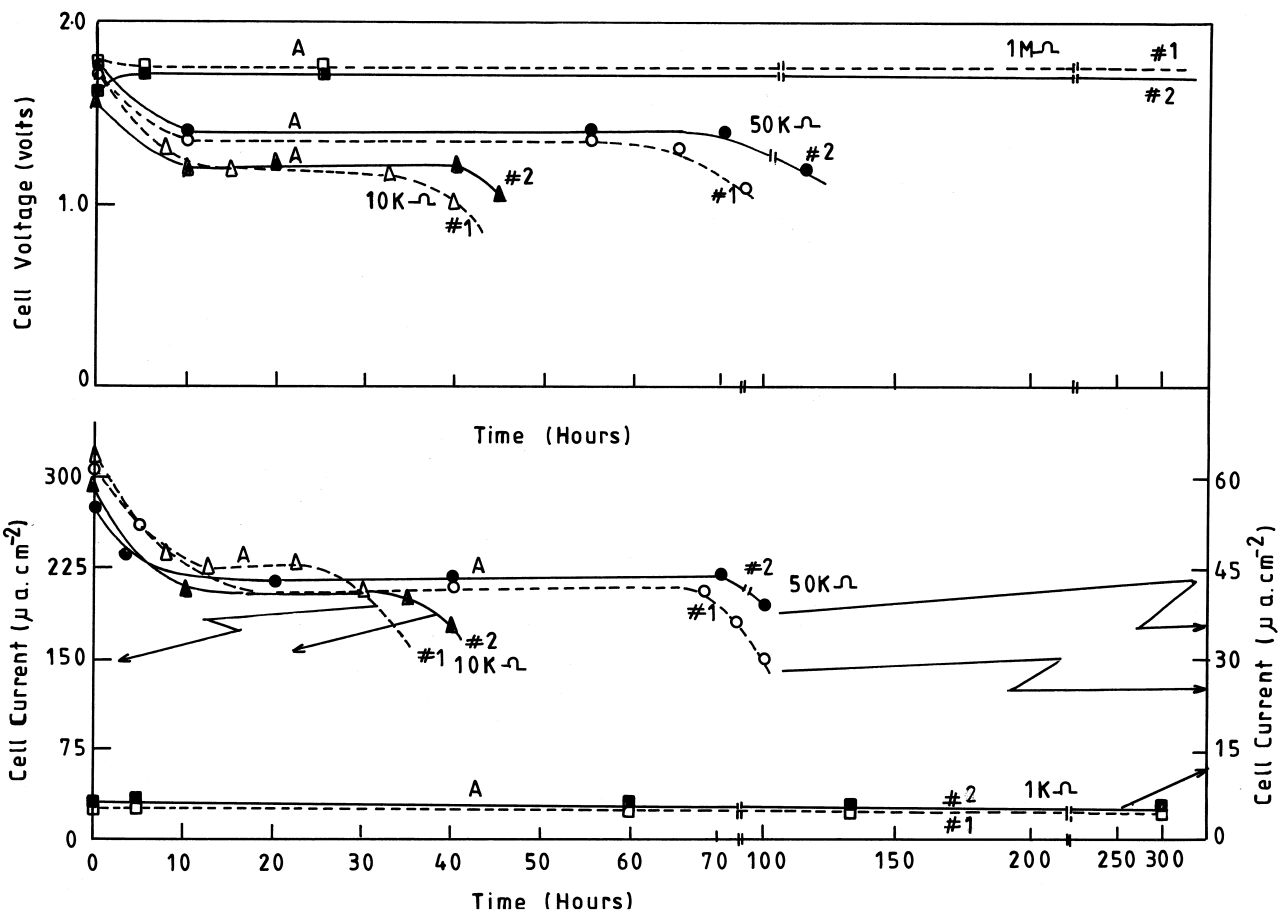

Fig. 3. Cell voltage and cell current vs. time plots for cell #1 [$Zn + ZnSO_4 \cdot 7H_2O//H_3PW_{12}O_{40} \cdot nH_2O + Al_2(SO_4)_3 \cdot 16H_2O//PbO_2 + V_2O_5 + C + E$ shown with open points and dashed lines (– ∘ ∘ –) and cell #2 [$Zn + ZnSO_4 \cdot 7H_2O$ + metal hydride$//H_3PW_{12}O_{40} \cdot nH_2O + Al_2(SO_4)_3 \cdot 16H_2O//PbO_2 + V_2O_5 + C + E$ shown as filled points and full lines (___ · · · ___) at loads 10 kΩ, 50 kΩ, and 1 mΩ.

Table 1
Open-circuit voltage (OCV) and current density in the stable performance region with 10 kΩ load, together with the duration of stable performance, for cells which illustrate the effect of changing the electrolyte from $H_3PW_{12}O_{40} \cdot nH_2O$ to $H_3PW_{12}O_{40} \cdot nH_2O + Al_2(SO_4)_3 \cdot 16H_2O$ composite

Anode:	Zn		$Zn + ZnSO_4 \cdot 7H_2O$		$Zn + ZnSO_4 \cdot 7H_2O$ + metal hydride	
Electrolyte	$H_3PO_412 \cdot WO_3 \cdot nH_20$	$0.5H_3PO_4 \cdot 12WO_3 \cdot nH_2O + 0.5Al_2(SO_4)_3 \cdot 16H_2O$	$H_3PO_412 \cdot WO_3 \cdot nH_2O$	$0.5H_3PO_4 \cdot 12WO_3 \cdot nH_2O + 0.5Al_2(SO_4)_3 \cdot 16H_2O$	$H_3PO_412 \cdot WO_3 \cdot nH_2O$	$0.5H_3PO_4 \cdot 12WO_3 \cdot nH_2O + 0.5Al_2(SO_4)_3 \cdot 16H_2O$
OCV (V)	1.70	1.77	1.73	1.71	1.54	1.74
Current density ($\mu A\ cm^{-2}$)	230	250	240	220	210	205
Time for stable performance (h)	2	20	4	24	6	28

Table 2
Performance of cells that highlights the effect of changing the anode composition for two different electrolytes ($H_3PW_{12}O_{40} \cdot nH_2O$ and $H_3PW_{12}O_{40} \cdot nH_2O + Al_2(SO_4)_3 \cdot 16H_2O$ composite)

Electrolyte	$H_3PO_412 \cdot WO_3 \cdot nH_2O$			$0.5H_3PO_4 \cdot 12WO_3 \cdot nH_2O + 0.5Al_2(SO_4)_3 \cdot 16H_2O$		
Anode:	Zn	$Zn + ZnSO_4 \cdot 7H_2O$	$Zn + ZnSO_4 \cdot 7H_2O +$ Metal hydride	Zn	$Zn + ZnSO_4 \cdot 7H_2O$	$Zn + ZnSO_4 \cdot 7H_2O +$ Metal hydride
OCV (V)	1.70	1.73	1.54	1.77	1.71	1.77
Current density ($\mu A\ cm^{-2}$)	230	240	210	250	220	205
Time for stable performance (h)	2	4	6	20	24	28

$ZnSO_4 \cdot 7H_2O$ + metal hydride), the addition of $Al_2(SO_4)_3 \cdot 16H_2O$ to $H_3PW_{12}O_{40} \cdot nH_2O$ electrolyte leads to an improvement in the duration of stable performance. Similarly, it may be noted from Table 2 that the time of stable performance is less when pure Zn is used as the anode and $H_3PW_{12}O_{40} \cdot nH_2O$ as the electrolyte. The stability increases with the addition of $ZnSO_4 \cdot 7H_2O$ and increases further with the addition of metal hydride. A similar trend is noticed when $H_3PW_{12}O_{40} \cdot nH_2O + Al_2(SO_4)_3 \cdot 16H_2O$ composite is used as the electrolyte. The anode composition Zn + $ZnSO_4 \cdot 7H_2O$ + metal hydride gives the best performance. The enhancement in the stable performance may be due to the following.

(i) Better compatibility of electrolyte because at the interface Zn may react with $Al_2(SO_4)_3 \cdot 16H_2O$ to give $ZnSO_4$ compatible with the bulk anode.

(ii) Copious supply of H^+ available from the metal hydride. We shall discuss some results later in which it will be shown that the addition of metal hydride also improves the rechargeability.

Another important observation which can be made from the discharge characteristics given in Fig. 3 is that the duration of stable performance is dependent upon the current drain. With a low current drain (2.5 $\mu A\ cm^{-2}$ at 1 $M\Omega$ load), the cell can perform for well over 300 h. This time decreases, however, as the current drain increases (viz., 60–70 h for 45 $\mu A\ cm^{-2}$ at 50 $k\Omega$ load; 24 to 28 h for 200 to 220 $\mu A\ cm^{-2}$ at 10 $k\Omega$ load). At high current drains (e.g., about 200 $\mu A\ cm^{-2}$ with 10 $k\Omega$ load in cell #2), if the operating time is taken beyond 24 h to more than 50 h then the cells are found to swell and, ultimately, the assembly pellets split. The swelling may be due to the entrapment of mobile protons in the electrolytes or in the layers of the intercalating cathode. The volume of intercalation compounds is known to increase on ion intercalation [15]. Under deep-discharge conditions, the mobile intercalating species (H^+ in this case) can no more be accommodated in the intercalating layers. This leads to swelling and build up of pressure at the interface as well as in the bulk. The splitting behaviour of the cell is shown schematically in Fig. 4a. The swelling of cathode and electrolyte is visible to the naked eye after ~75 h for a 10 $k\Omega$ load. The cell cracked or split after about 200 h. During the process of discharge, a change in the cell resistance is expected. Complex-impedance plots for the initial and sufficiently discharged cell (~150 h, swollen but not split) are given in Fig. 4b. As expected, the bulk resistance increases from 2.5×10^3 to $1.6 \times 10^5\ \Omega$ and the electrode–electrolyte resistance increases from 3.6×10^3 to $3.0 \times 10^5\ \Omega$.

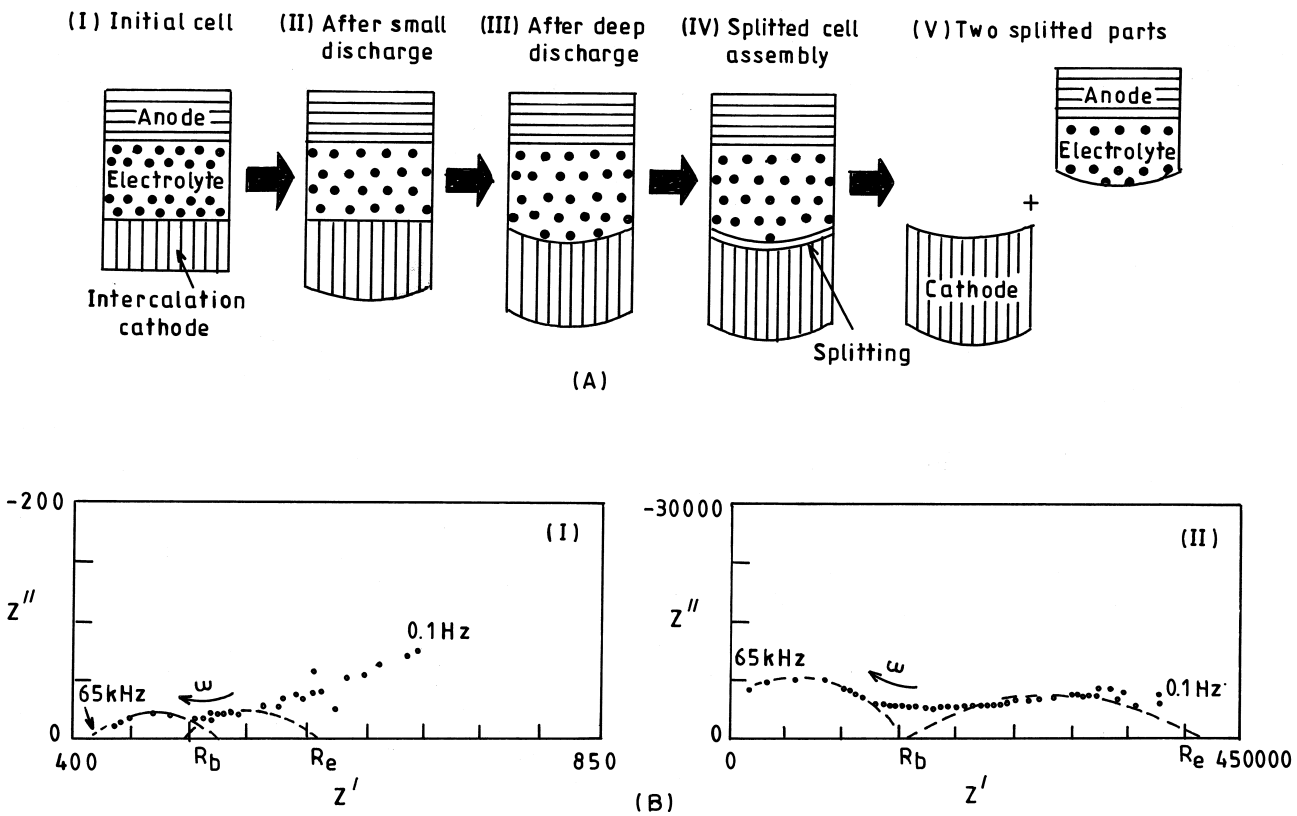

Fig. 4. (a) Schematic representation of changes in the physical structure of the cell at different stages of discharge. (b) Complex-impedance plot of initial cell (I) and after sufficient discharge but before splitting of cell (II).

3.3. Rechargeability of cells

Typical rechargeability behaviour of cells #1 and #2 is given in Fig. 5. In order to perform this experiment, the voltage–current characteristics of the cell were measured while discharging through a 50-kΩ load for a time, t. The discharge experiment was terminated after the cell voltage dropped by 10%. The cell was then recharged by connecting it to a constant-current source. During charging, the same amount of charge was supplied which was withdrawn during discharging. The time t' for which charging is to be carried out can be calculated using the following expression:

$$i_{\text{charging}} \times t' = i_{\text{av. discharge}} \times t$$

It is clear from Fig. 5a that the rechargeability can be attained without much loss of voltage or current. The voltages attained after different charge cycles are given in Fig. 5b. Cells #1 and #2 can be recharged for $\sim$20 and 30 cycles, respectively. The superior rechargeability of cell #2 is possibly due to the presence of metal hydride in its anode compartment. This ensures the possibility of hydrogen supply. Since the rechargeability behaviour is linked closely with the intercalation of H^+ in the cathode, the name 'Proton Battery' has been given to our cell. It should also be noted that the electrolyte used is a well-established proton conductor [16] and does not conduct ions like Zn^{2+}, etc. The intercalation of H^+ in V_2O_5 has been studied in detail by Dickens et al. [17] and Chippendale and Dickens [18] who gave the following intercalation reaction:

$$1/xV_2O_5 + H^+ + e^- = 1/xH_xV_2O_5$$

In 1987, Ritter [19] showed that since hydrogen is the smallest ion it has a greater intercalation efficiency than other ions. At room temperature, insertion of up to 3.8 H^+ ions has been reported in α-V_2O_5. An interesting experi-

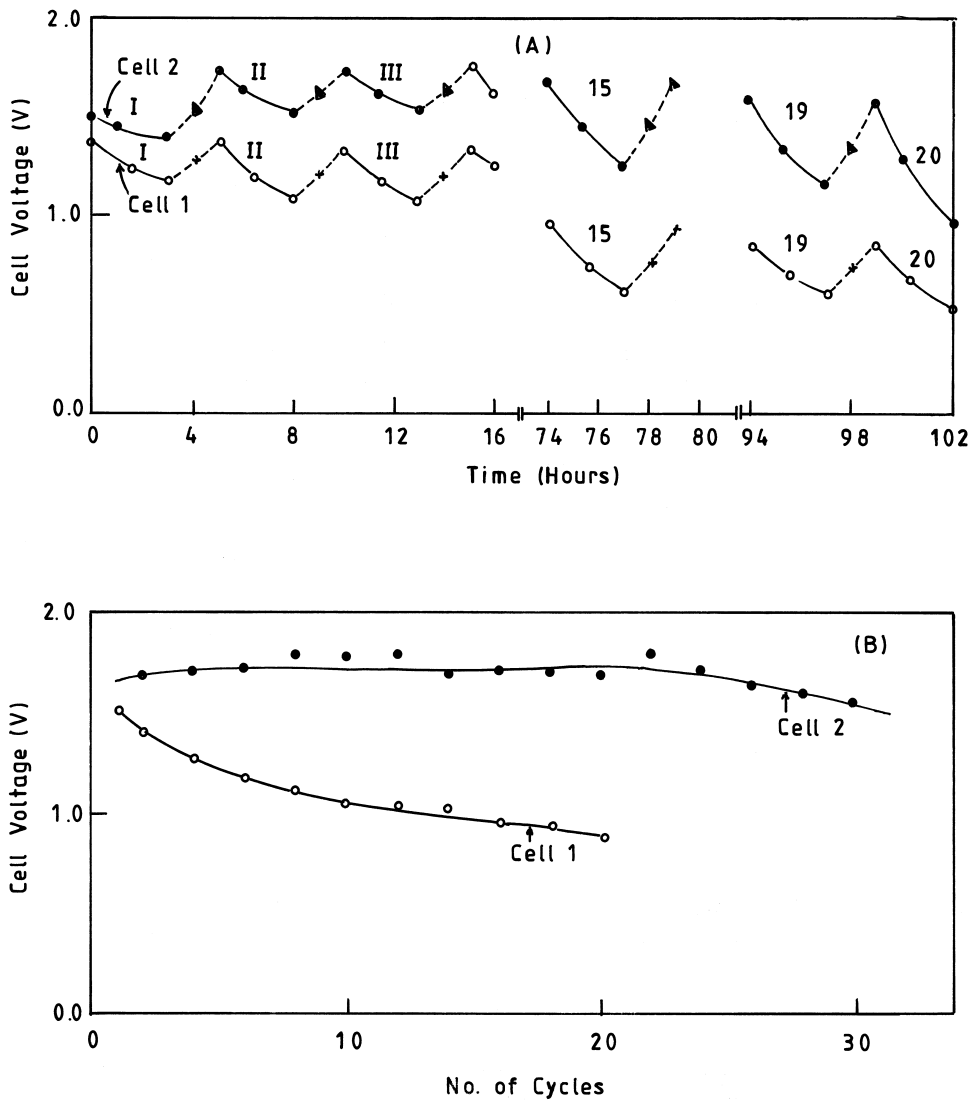

Fig. 5. (a) Cell voltage as a function of time during different charge–discharge cycles for cells #1 and #2. (b) Cell voltages after different 'charge' cycles as a function of the number of charging cycles for cells #1 and #2.

ment has been reported by Schollhorn and Kuhlman [20] in which V_2O_5 intercalation was examined in an aqueous solution of different salts. It was concluded that H^+ (and not other larger cations) are intercalated. In this experiment, though medium-sized cations Na^+, Ca^{2+}, Zn^{2+} were present, they did not show any tendency to form insertion compounds. From all this discussion, it can be summarized that mobile protons (H^+) from the electrolyte intercalate (and de-intercalate) in our cathode compartment and play a dominant role in the rechargeability of the battery.

4. Conclusions

A rechargeable proton battery can be fabricated using an anode which supplies H^+ ions, a proton conductor, and an intercalating cathode. A possible cell has the configuration: $Zn + ZnSO_4 7H_2O + \text{Metal hydride}//H_3PW_{12}O_{40} \cdot nH_2O + Al_2(SO_4)_3 \cdot 16H_2O//PbO_2 + V_2O_5 + C + E$. Addition of metal hydride in the anode and the use of $H_3PW_{12}O_{40} \cdot nH_2O + Al_2(SO_4)_3 \cdot 16H_2O$ composite instead of pure phosphotungstic acid have been shown to improve the cell performance.

Acknowledgements

Thanks are due to the Ministry of Non-Conventional Energy Sources for providing the funding. KP and NL are grateful to CSIR (India) for granting a Research Associateship and a SRF, respectively. Thanks are also due to Professor O.N. Srivastava for providing the metal hydride.

References

[1] C. Julien, G.A. Nazri, Solid State Batteries: Materials Design and Optimization, Kluwer Academic Publishers, London, 1994.
[2] M.Z.A. Munshi (Ed.), Handbook of Solid State Batteries and Capacitors, World Scientific, Singapore, 1995.
[3] S. Chandra, Superionic Solids—Principles and Applications, North Holland, Amsterdam, 1981.
[4] Ph. Colomban (Ed.), Proton Conductors: Solids Membranes and Gels Materials and Devices, Cambridge Univ. Press, New York, 1992.
[5] S. Chandra, in: A.L. Laskar, S. Chandra (Eds.), Superionic Solid and Solid Electrolytes—Recent Trends, Academic Press, New York, 1989, p. 185.
[6] C. Poinsignon, Mater. Sci. Eng. B 3 (12) (1989) 37.
[7] J. Guitton, B. Dongui, R. Mosdale, M. Foresteir, in: W. Weppener, H. Schulz (Eds.), Solid State Ionics—87, North Holland, 1988, p. 847.
[8] H. Kahil, M. Foresteir, J. Guitton, in: J. Jenson (Ed.), Solid State Protonic Conductors III La Grande Motte (France), Odense University Press, 1984, p. 84.
[9] S. Chandra in Ref. 2, p. 579.
[10] A.Kr. Singh, A.K. Singh, O.N. Srivastava, Int. J. Hydrogen Energy 18 (1993) 567.
[11] R.C.T. Slade, J. Barker, T.K. Halstead, Solid State Ionics 24 (1987) 571.
[12] S.A. Hashmi, D.K. Rai, S. Chandra, J. Mater. Sci. 27 (1992) 175.
[13] J. Maier, in: S. Chandra, A.L. Laskar (Eds.), Superionic Solids and Solid Electrolytes: Recent Trends, Academic Press, New York, 1989, p. 137.
[14] J.B. Wagner Jr., C. Wagner, J. Chem. Phys. 26 (1957) 1597.
[15] C.A.C. Sequeira, in: C.A.C. Sequeira, A. Hooper (Eds.), Solid State Batteries, Martinus Nijhoff Publishers, 1985, p. 241.
[16] K. Pandey, S. Chandra, to be communicated.
[17] P.G. Dickens, A.M. Chippindale, S.J. Hibble, Solid State Ionics 34 (1989) 79.
[18] A.M. Chippendale, P.G. Dickens, Solid State Ionics 23 (1987) 183.
[19] C. Ritter, Z. Phys. Chem. 151 (1987) 51.
[20] R. Schollhorn, R. Kuhlman, Mater. Res. Bull. 11 (1976) 83.